Journal of Power Sources 246 (2014) 356–360

Contents lists available at ScienceDirect

Journal of Power Sources

journal homepage: www.elsevier.com/locate/jpowsour

Short communication

Oleylamine-functionalized palladium nanoparticles with enhanced electrocatalytic activity for the oxygen reduction reaction

Yi Shi, Shengkang Yin, Yanrong Ma, Dingkun Lu, Yu Chen, Yawen Tang*, Tianhong Lu

Jiangsu Key Laboratory of New Power Batteries, Jiangsu Collaborative Innovation Center of Biomedical Functional Materials, College of Chemistry and Materials Science, Nanjing Normal University, 1# Wenyuan Road, Nanjing 210023, PR China

HIGHLIGHTS

- Monodisperse oleylamine-stablized Pd nanoparticles (Pd–OAm) are synthesized.
- Low cost $Pd(Ac)_2$ is a promising precursor for Pd nanoparticles synthesis.
- Pd–OAm shows superior electrocatalytic activity for the ORR.
- Pd–OAm possesses excellent formic acid-tolerant ability.

GRAPHICAL ABSTRACT

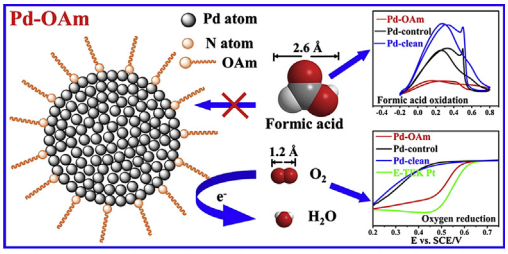

Oleylamine (OAm) functionalized palladium nanoparticles showed an enhanced electrocatalytic activity and formic acid tolerance for the oxygen reduction reaction.

ARTICLE INFO

Article history:
Received 24 May 2013
Received in revised form
24 July 2013
Accepted 28 July 2013
Available online 3 August 2013

Keywords:
Oleylamine
Palladium
Surface functionalization
Oxygen reduction reaction
Formic acid oxidation reaction

ABSTRACT

The oleylamine (OAm)-functionalized Pd nanoparticles (Pd–OAm) have been conveniently synthesized through direct thermal decomposition method of low cost palladium acetate. The morphology, crystalline structure and composition of the Pd–OAm are investigated by transmission electron microscopy (TEM), X-ray diffraction (XRD) and X-ray photoelectron spectroscopy (XPS). Fourier transform infrared (FT-IR) spectroscopy, XPS and zeta potential analysis confirm the successful immobilization of OAm molecules on the Pd nanoparticles surface. The Pd–OAm displays an enhanced electrocatalytic activity and formic acid-tolerant ability for the oxygen reduction reaction (ORR), suggesting a potential application in cathodic catalyst for direct formic acid fuel cells.

1. Introduction

The oxygen reduction reaction (ORR) at Pt cathodic catalysts is a very important reaction in low-temperature polymer electrolyte membrane fuel cells (LPEMFCs), such as proton-exchange membrane fuel cells (PEMFCs), direct methanol fuel cells (DMFCs) and direct formic acid fuel cells (DFAFCs) [1,2]. However, the scarcity and high cost of Pt have seriously impeded the commercialization of LPEMFCs [3–5]. Although Pd is the most Pt-like metal and has a relatively abundant resource, the single-component Pd catalysts exhibit less electrocatalytic activity for the ORR compared with Pt catalysts. To address this issue, tremendous efforts have been dedicated to improving the existing Pd catalysts in the past decades, including tailoring the morphology of Pd nanoparticles, fabricating advanced Pd catalysts with bimetallic/intermetallic compositions and core–shell structures, etc. [6–9].

In the conventional opinion, the capping agents in wet-chemistry synthesis were previously considered to hamper

* Corresponding author. Tel.: +86 25 85891651; fax: +86 25 83243286.
E-mail address: tangyawen@njnu.edu.cn (Y. Tang).

0378-7753/$ – see front matter © 2013 Elsevier B.V. All rights reserved.
http://dx.doi.org/10.1016/j.jpowsour.2013.07.099

the electrocatalytic activity of metal nanoparticles, and were usually removed to leave the "clean" chemically/electrochemically active sites [10–12]. For example, Sun and Mazumder antecedently reported a facile synthesis of monodisperse Pd nanoparticles by the reduction of palladium(II) acetylacetonate in the presence of oleylamine and borane tributy-lamine complex [10]. The oleylamine-coated Pd nanoparticles were further "cleaned" by an acetic acid wash procedure. As a result, the pre-treated Pd nanoparticles displayed excellent electrocatalytic activity and stability for the formic acid oxidation reaction. Recently, there emerged another novel route to tune electrocatalytic activity of Pt catalysts for the ORR, which was based on the surface modification of the Pt metal by nonmetallic molecules that could block the adsorption of poisoning species and spectator anions [13] or influence the electronic property of the Pt atom [14]. For example, the ORR activity on cyanide (CN^-) modified Pt facets showed a 25-fold increase in the H_2SO_4 solution compared to naked Pt facets due to the suppression of SO_4^{2-} ion adsorption [13]. The polyallylamine-functionalized Pt nanocubes with {100} facets exhibited superior electrochemical activity for the ORR in both H_2SO_4 and $HClO_4$ solutions compared to the commercial Pt black due to the electronic effect [14]. These facts indicated that appropriate surface modification of metal nanoparticles may improve their electrocatalytic activity for the particular electrochemical reaction.

In this communication, oleylamine (OAm) was applied to prepare OAm-functionalized Pd nanoparticles (Pd–OAm) through direct thermal decomposition method of palladium acetate. The resultant Pd–OAm possessed markedly enhanced electrocatalytic activity for the ORR and very low electrocatalytic activity for the formic acid oxidation reaction.

2. Experimental

2.1. Preparation of oleylamine-functionalized Pd nanoparticles (Pd–OAm)

In a typical synthesis, 126.6 mg palladium acetate was dissolved in 12 mL of N_2-saturated octadecylene/OAm mixture with a volume ratio of 5:1 at 50 °C. Under vigorous stirring, the mixture was heated to 200 °C for 2 h. After being cooled to room temperature, the black Pd–OAm catalyst was separated by centrifugation at 20,000 rpm for 10 min, washed several times with ethanol, and then dried at 60 °C for 5 h in a vacuum dryer. For comparison, Pd nanoparticles (termed as Pd-control) were also prepared using similar procedure in the absence of OAm. Meanwhile, Pd nanoparticles with "clean" surface (termed as Pd-clean) were synthesized by washing Pd–OAm catalyst with acetic acid [10].

2.2. Characterization

The morphology, structure and composition of the catalysts were characterized by Fourier transform infrared (FT-IR) spectrometer (Nicolet 520-SX FT-IR), zeta potential analyzer (Malvern Zetasizer Nano ZS90), transmission electron microscopy (TEM, JEOL JEM-2100F), X-ray diffraction (XRD, Model D/max-rC X-ray diffractometer), and X-ray photoelectron spectroscopy (XPS, Thermo VG Scientific ESCALAB 250 spectrometer). The binding energy was calibrated by means of the C 1s peak energy of 284.6 eV. All electrochemical experiments were performed on a CHI 660 C electrochemical analyzer at 30 ± 1 °C. A standard three-

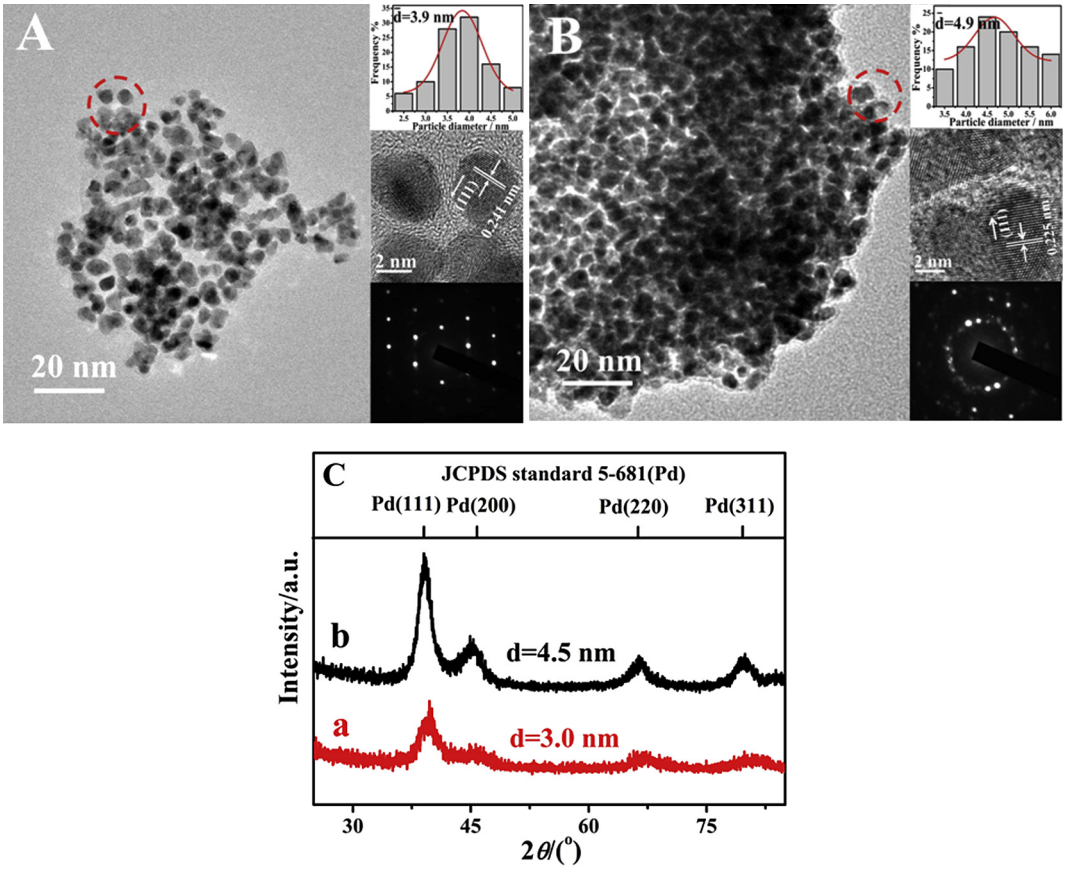

Fig. 1. (A) TEM image of Pd–OAm. Inset in A: corresponding particle size distribution histogram (up), HRTEM image (middle) and SAED image (bottom). (B) TEM image of Pd-control. Inset in B: corresponding particle size distribution histogram (up), HRTEM image (middle) and SAED image (bottom). (C) XRD patterns of (a) Pd–OAm and (b) Pd-control.

electrode system was used including a Pt wire auxiliary electrode, a saturated calomel reference electrode (SCE), and a catalyst modified glassy carbon electrode as the working electrode. All potentials in this study were reported with respect to SCE. The working electrode was prepared according to literature [15]. The specific metal loading of all catalysts (homemade Pd catalysts and commercial E-TEK Pt black) on the electrode surface was about 140 μg cm^{-2}.

2.3. Measurement of the electrochemically active surface area

Cyclic voltammetry (CV) measurements were carried out in N_2-saturated 0.1 M $HClO_4$ solutions at a sweep rate of 50 mV s^{-1}. The electrochemically active surface area (ECSA) of Pd catalysts was calculated from CVs in 0.1 M $HClO_4$ solution by integrating the reduction charge of surface $Pd(OH)_2$ and assuming a value of 420 μC cm^{-2} for the reduction charge of a $Pd(OH)_2$ monolayer on the Pd surface [7]. The ECSA of Pt black was also calculated from CVs in 0.1 M $HClO_4$ solution by measuring the charge collected in the hydrogen adsorption/desorption region after double-layer correction and assuming a value of 210 μC cm^{-2} for the adsorption of a hydrogen monolayer [16].

2.4. Electrochemical parameters of the oxygen reduction reaction

The oxygen reduction reaction (ORR) measurements were conducted at room temperature in 0.1 M $HClO_4$ solution under a flow of O_2 using the rotating disk electrode (RDE) at a rotation rate of 2000 rpm and a sweep rate of 10 mV s^{-1}. Based on the ORR polarization curves, the kinetic current (I_k) was corrected using (Eq. (1)), which was described as follows:

$$\frac{1}{I} = \frac{1}{I_k} + \frac{1}{I_L} \quad (1)$$

where I_L and I were the limited diffusion current and the measured current, respectively. Specific kinetic activities of catalysts toward the ORR were investigated by converting I_k into kinetic current densities i_k (dividing by the true ECSA area).

3. Results and discussion

The morphologies of Pd–OAm and Pd-control were investigated by TEM. The spherical Pd–OAm has good dispersion (Fig. 1A). According to distribution histogram, the average particle size of Pd–OAm is estimated to be 3.9 nm (up-inset). The high-resolution TEM (HRTEM) data yield an interfringe distance of 0.241 nm (middle-inset), in good agreement with the lattice spacing of the {111} facets of the face-centered cubic (*fcc*) Pd crystal (0.225 nm), indicating that Pd–OAm mainly consists of Pd{111} facets. The selected area electron diffraction (SAED) pattern shows not only continuous rings but also discrete diffraction spots (bottom-inset), indicating that each Pd–OAm nanoparticles have a polycrystalline structure. For Pd-control sample, HRTEM image and SAED pattern show Pd-control mainly consists of Pd{111} facets and has a polycrystalline structure (insets in Fig. 1B), similar to Pd–OAm sample. However, TEM image and corresponding distribution histogram show Pd-control with 4.9 nm size has a heavy agglomeration (Fig. 1B and inset). The XRD pattern shows that both Pd–OAm and Pd-control have *fcc* structure (JCPDS standard 5-681 (Pd)) (Fig. 1C). According to the Scherrer equation, the average particle size of Pd–OAm and Pd-control are calculated to be 3.0 nm and 4.5 nm, respectively, in consistent with the values measured from TEM images. TEM

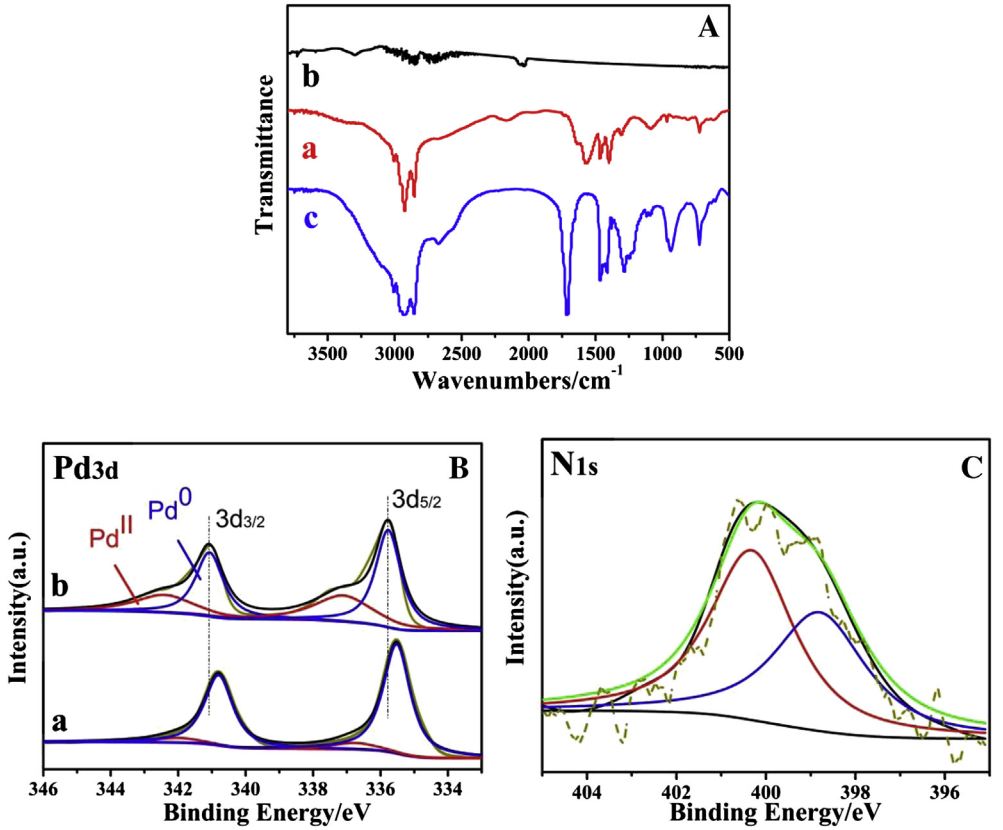

Fig. 2. (A) FT-IR spectra of (a) Pd–OAm, (b) Pd-control and (c) pure OAm. (B) XPS spectra of (a) Pd–OAm and (b) Pd-control in the Pd 3d region. (C) XPS spectrum of Pd–OAm in the N 1s region.

observation and XRD analysis clearly indicate that OAm can prevent the aggregation of Pd nanoparticles and reduce the average size of particles effectively. In our synthesis, the price of palladium acetate precursor is only about one-third that of widely used palladium(II) acetylacetonate precursor during Pd nanoparticles synthesis [8,10,17]. However, the dispersion and particle size of as-prepared palladium acetate are comparable to the Pd nanoparticles obtained by using palladium(II) acetylacetonate as reaction precursor [8,10,17]. Obviously, the present thermal decomposition method of palladium acetate is an attractive choice for the synthesis of Pd nanoparticles.

The surface composition of Pd–OAm was investigated by FT-IR, zeta potential and XPS. The FT-IR spectrum of Pd–OAm is similar to that of pure OAm (Fig. 2A), indicating OAm wraps on the surface of Pd nanoparticles. Note that the zeta potential of Pd–OAm is +16.8 mV (pH = 7), further confirming the immobilization of OAm on Pd nanoparticles surface. Thus, the electrostatic repulsion can prevent the aggregation of Pd nanocrystals during synthesis, resulting in good dispersivity and uniformity. XPS measurements display the content of Pd^0 species in Pd–OAm is much higher than that of Pd-control (91% vs. 58%), demonstrating the excellent oxidation resistance of Pd–OAm (Fig. 2B). Moreover, the binding energy values of Pd^0 and Pd^{II} species in Pd–OAm negatively shift ca. 0.3 eV compared to that of Pd-control, which indicates that the capping of OAm on Pd nanoparticles can result in a change in Pd 3d binding energy due to a strong Pd–N interaction [18]. In order to further prove the formation of Pd–N bond, the N 1s spectrum was also analyzed. The N 1s peak is deconvoluted into two components (Fig. 2C). The binding energy of 400.2 eV corresponds to N 1s peak of free $-NH_2$ groups and the other peak at 398.8 eV is assigned to N atom bound on Pd surface [19].

Fig. 3A shows the cyclic voltammograms of electrocatalysts in 0.1 M $HClO_4$ solution. It is clearly observed that the onset potentials for surface oxide formation ($Pd + H_2O \rightarrow Pd - OH + H^+ + e^-$) and the following reduction on Pd–OAm positively shift ca. 60 mV compared to Pd-control, suggesting Pd–OAm restrains the chemisorption of OH on the Pd sites at high potential. After washing Pd–OAm with acetic acid [10], the onset oxidation surface potential on the obtained Pd-clean is very close to that on Pd-control, indicating OAm on Pd nanoparticles plays an important role in enhancing anti-oxidation ability of Pd–OAm. By calculation, the ECSA of Pd–OAm, Pd-control, Pd-clean and E-TEK Pt are measured to be 4.15, 13.88, 20.31 and 15.07 $m^2\ g^{-1}$, respectively (see Experimental section for calculation details). Fig. 3B shows the typical ORR polarization curves for electrocatalysts in O_2-saturated 0.1 M $HClO_4$ solution. The current density is normalized to the geometrical area of the glassy carbon electrode. ORR onset potentials of Pd–OAm, Pd-control and Pd-clean are 0.61, 0.44 and 0.45 V, respectively. The electrochemical results clearly demonstrate that OAm-functionalization of Pd nanoparticles can markedly enhance the ORR activity of Pd nanoparticles. Since adsorbed hydroxyl species inhibit the ORR, the excellent anti-oxidation ability of Pd–OAm surface may facilitate the ORR kinetics. Moreover, Pd 3d binding energy value of Pd–OAm negatively shift ca. 0.3 eV compared to that of Pd-control (see Fig. 2B), which decreases the adsorption strength of oxygen on Pd substrate and thus improves ORR activity, according to d-band centre theory [20]. Finally, it is observed that Pd–OAm exhibits good potential to close the gap with the state-of-the-art E-TEK Pt (0.61 V vs. 0.64 V), making Pd–OAm a promising cathodic electrocatalyst. The specific kinetic current density (i_k) represents the intrinsic activity of catalysts, which is a better indicator of an electrocatalysts' quality. To further reflect

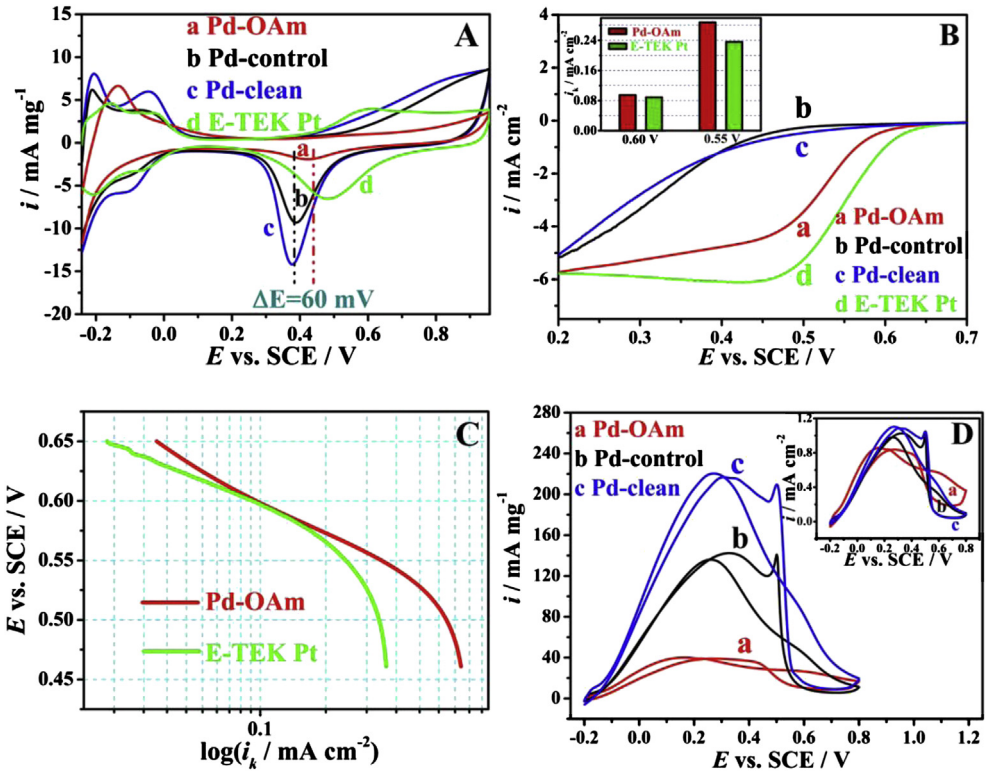

Fig. 3. (A) Cyclic voltammograms of (a) Pd–OAm, (b) Pd-control, (c) Pd-clean and (d) E-TEK Pt catalysts in 0.1 M $HClO_4$ solution at the rate of 50 mV s^{-1}. (B) ORR polarization curves obtained in an O_2-saturated 0.1 M $HClO_4$ solution. ORR measurements were conducted by using a GC RDE at a rotation rate of 2000 rpm and a sweep rate of 10 mV s^{-1}. Inset: Specific kinetic current densities (i_k) of electrocatalysts at a fixed potential of 0.55 V and 0.60 V for the ORR. (C) Mass transfer-corrected E vs. log i_k (Tafel) plots for Pd–OAm and E-TEK Pt catalysts in an O_2-saturated 0.1 M $HClO_4$ solution (i_k is kinetic current density per Pd or Pt electroactive area). (D) Cyclic voltammograms in N_2-saturated 0.1 M $HClO_4$ + 0.5 M HCOOH solution. Inset: specific activity of electrocatalysts for formic acid oxidation.

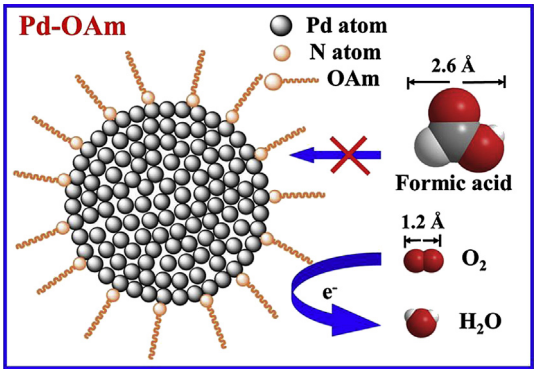

Scheme 1. Schematic representation of the influence of OAm barrier networks at Pd–OAm surface on the accessibility of formic acid molecule with big molecule size.

electrochemical activity toward the ORR, specific kinetic activities were inserted in Fig. 3B. As seen, the i_k value for Pd–OAm is even slightly superior to that of E-TEK Pt at 0.55 V and 0.60 V, further confirming excellent catalytic activity of Pd–OAm toward the ORR.

Based on these results, mass transfer-corrected E vs. log i_k plots were constructed and they are shown in Fig. 3C, whereby the kinetic current density i_k was calculated on the basis of electroactive Pd or Pt area. In the low current density region (between 0.60 and 0.55 V), the values of the Tafel slopes for Pd–OAm and E-TEK Pt were −74 and −71 mV dec^{-1} respectively, which were slightly higher than the value of −60 mV dec^{-1} expected for bulk polycrystalline Pd and Pd nanocatalysts [21]. In the high current density region (between 0.35 and 0.40 V), the Tafel slope values >380 mV dec^{-1} were found for Pd–OAm and E-TEK Pt, which are considerably higher than −120 mV dec^{-1} that is usually observed for Pd electrodes in this potential region [21]. In view of the above-mentioned facts, the catalyst activity is found to vary as: Pd–OAm > E-TEK Pt, which is akin to that observed from the specific kinetic current density.

The development of formic acid-tolerant cathodic electrocatalyst is a critical challenge for direct formic acid fuel cells because the crossover of formic acid from anode side causes a mixed potential at the cathode side to damage the cell. Here, formic acid tolerance of Pd–OAm was evaluated by cyclic voltammetry (Fig. 3D). It is observed that peak current of Pd–OAm is much lower than that of Pd-control and Pd-clean. In order to further investigate the intrinsic electrocatalytic activity of the catalyst, the specific kinetic activity (normalized to ECSA) was also shown. As observed, the peak current density (i.e., the specific activity) of the formic acid oxidation on Pd–OAm is still lower than that of Pd-control and Pd-clean, indicating Pd–OAm has excellent formic acid-tolerant ability.

We ensure that OAm on Pd nanoparticles can act as barrier networks to inhibit the accessibility of formic acid on Pd surface because that molecule size of formic acid molecule is 2.2 times bigger than that of O_2 molecule, as is shown in Scheme 1. Meanwhile, O_2 molecule is hydrophobic whereas HCOOH is a polar molecule. According to similar compatible principle, the permeation of hydrophobic O_2 in CH_2 chains of OAm molecules is easier than that of HCOOH, which endows Pd–OAm with particular selectivity for the ORR.

4. Conclusion

In summary, the monodisperse Pd–OAm was conveniently synthesized through direct thermal decomposition of palladium acetate in the presence of OAm, indicating the low cost palladium acetate was a promising Pd^{II} precursor for synthesis of Pd nanostructures. Due to the change in Pd electronic structure and steric blocking effect of OAm adsorption layers, Pd–OAm showed excellent electrocatalytic activity and formic acid tolerance for the ORR in acidic media. The present experimental result demonstrated that the surface modification of the Pd nanoparticles is also a promising strategy to improve their electrocatalytic activity and selectivity for the ORR.

Acknowledgments

The authors are grateful for the financial support of NSFC (21073094 and 21273116), the United Fund of NSFC and Yunnan Province (U1137602), Industry-Academia Cooperation Innovation Fund Project of Jiangsu Province (BY2012001), Natural Science Foundation of Jiangsu Province (SBK201320448), and a project funded by the Priority Academic Program Development of Jiangsu Higher Education Institutions.

References

[1] R. Lin, C. Cao, T. Zhao, Z. Huang, B. Li, A. Wieckowski, J. Ma, J. Power Sources 223 (2013) 190–198.
[2] M. Oezaslan, P. Strasser, J. Power Sources 196 (2011) 5240–5249.
[3] F. Su, C.K. Poh, J. Zeng, Z. Zhong, Z. Liu, J. Lin, J. Power Sources 205 (2012) 136–144.
[4] Y. Tang, H. Zhang, H. Zhong, T. Xu, H. Jin, J. Power Sources 196 (2011) 3523–3529.
[5] R. Yang, W. Bian, P. Strasser, M.F. Toney, J. Power Sources 222 (2013) 169–176.
[6] L. Zhang, F. Hou, Y.W. Tan, Chem. Commun. 48 (2012) 7152–7154.
[7] L. Xiao, L. Zhuang, Y. Liu, J. Lu, H.c.D. Abruna, J. Am. Chem. Soc. 131 (2008) 602–608.
[8] R. Rego, C. Oliveira, A. Velazquez, P.L. Cabot, Electrochem. Commun. 12 (2010) 745–748.
[9] H. Erikson, A. Sarapuu, K. Tammeveski, J. Solla-Gullon, J.M. Feliu, Electrochem. Commun. 13 (2011) 734–737.
[10] V. Mazumder, S. Sun, J. Am. Chem. Soc. 131 (2009) 4588–4589.
[11] J. Zhang, H. Yang, J. Fang, S. Zou, Nano Lett. 10 (2010) 638–644.
[12] C. Wang, H. Daimon, T. Onodera, T. Koda, S. Sun, Angew. Chem. 120 (2008) 3644–3647.
[13] D. Strmcnik, M. Escudero-Escribano, K. Kodama, V.R. Stamenkovic, A. Cuesta, N.M. Markovic, Nat. Chem. 2 (2010) 880–885.
[14] G. Fu, K. Wu, X. Jiang, L. Tao, Y. Chen, J. Lin, Y. Zhou, S. Wei, Y. Tang, T. Lu, X. Xia, Phys. Chem. Chem. Phys. 15 (2013) 3793–3802.
[15] J. Xu, G. Fu, Y. Tang, Y. Zhou, Y. Chen, T. Lu, J. Mater. Chem. 22 (2012) 13585–13590.
[16] B. Lim, M. Jiang, P.H.C. Camargo, E.C. Cho, J. Tao, X. Lu, Y. Zhu, Y. Xia, Science 324 (2009) 1302–1305.
[17] T.Y. Jeon, S.J. Yoo, H.Y. Park, S.K. Kim, S. Lim, D. Peck, D.H. Jung, Y.E. Sung, Langmuir 28 (2012) 3664–3670.
[18] G. Fu, W. Han, L. Yao, J. Lin, S. Wei, Y. Chen, Y. Tang, Y. Zhou, T. Lu, X. Xia, J. Mater. Chem. 22 (2012) 17604–17611.
[19] S.W. Won, J. Park, J. Mao, Y.S. Yun, Bioresour. Technol. 102 (2011) 3888–3893.
[20] F.H.B. Lima, J. Zhang, M.H. Shao, K. Sasaki, M.B. Vukmirovic, E.A. Ticianelli, R.R. Adzic, J. Phys. Chem. C 111 (2007) 404–410.
[21] L.M. Vracar, D.B. Sepa, A. Damjanovic, J. Electrochem. Soc. 133 (1986) 1835–1839.